Circular Smooth Muscle Contractility Causes the Gut to Grow Anisotropically

Diana Khalipina[1#], Yusuke Kaga[1#], Nicolas Dacher[1], Nicolas R. Chevalier[*,1]

[1] Laboratoire Matière et Systèmes Complexes, Université Paris Diderot/CNRS UMR 7057, Sorbonne Paris Cité, 10 rue Alice Domon et Léonie Duquet, 75013 Paris, France

* Corresponding author : nicolas.chevalier@univ-paris-diderot.fr

[#] These authors contributed equally

This is the author's PDF version of the final article published in:

Khalipina D, Kaga Y, Dacher, N, Chevalier NR. 2019 Smooth muscle contractility causes the gut to grow anisotropically. J. R. Soc. Interface 16: 20190484. https://doi.org/10.1098/rsif.2019.0484

Abstract

The intestine is the most anisotropically-shaped organ, but, when grown in culture, embryonic intestinal stem cells form star- or sphere-shaped organoids. Here, we present evidence that spontaneous tonic and phasic contractions of the circular smooth muscle of the embryonic gut cause short-time scale elongation of the organ by a purely mechanical, self-squeezing effect. We present an innovative culture setup to achieve embryonic gut growth in culture and demonstrate by three different methods (embryological, pharmacological and microsurgical) that gut elongational growth is compromised when smooth muscle contractions are inhibited. We conclude that the cumulated short-term mechanical deformations induced by circular smooth muscle lead to long-term anisotropic growth of the gut, thus demonstrating a self-consistent way by which the function of this organ (peristalsis) directs its shape (morphogenesis). Our model correctly predicts that longitudinal smooth muscle differentiation later in embryogenesis slows down elongation, and that several mice models with defective gut smooth muscle contractility also exhibit gut growth defects. We lay out a comprehensive scheme of forces acting on the gut during embryogenesis and of their role in the morphogenesis of this organ. This knowledge will help design efficient in-vitro organ growth protocols and handle gut growth pathologies such as Short Bowel Syndrome.

Significance Statement

The intestine is a very long organ, 7 m on average in the human adult, and only a few centimeters in diameter. Its high aspect ratio increases the adsorption surface of the organ and allows for digestion to

proceed serially, in distinct chemical environments. By what mechanism does it grow to achieve these spectacular dimensions? Working on chicken embryos, we find that spontaneous peristaltic contractions of the circular smooth muscle constantly knead the proliferating embryonic intestinal tissue, making it elongate like play-doe. In contrast, non-contractile guts or spherically symmetric organoids grow isotropically. This research shows a consistent way by which the mechanical function of an organ (peristalsis) drives its shape (morphogenesis), and holds great promise to engineer functional intestinal organoids.

Introduction

Stem-cell derived intestinal organoids (1) form sphere- or star-shaped(2) structures instead of tubes. This observation shows that molecular information contained within the stem cells is not sufficient to trigger uniaxial anisotropic growth, making it necessary to factor in geometrical and mechanical cues (3) to fully understand organogenesis. Muscle contractility has been shown to be an essential actor of bone growth(4), lung branching(5), epithelial fold formation in the gut(6–9), oviduct(10), and even whole body-elongation in *C. Elegans* (11). We (12) and others (13) have shown that prolonged static longitudinal mechanical stress causes elongational growth of the gut. In this previous report (12), the mechanical stress we applied mimicked the in-vivo force exerted by the vitelline duct on the herniating early (E6-E9) embryonic gut loop. In this report, we elucidate how force generated by smooth muscle within the gut directs the growth of this organ.

The intestine presents at an early stage (day 6-7 of development in the chicken, week 7 in the human (14)) structural anisotropies at several levels: 1°) it is geometrically anisotropic, 2°) it has anisotropic non-muscle (passive) mechanical properties because collagen fibers wind circumferentially around the gut tract (15), 3°) it has anisotropic active contractile properties due to the presence of a circular smooth muscle (CSM) ring. CSM contractility has both static (muscle tone) and phasic components. Phasic contractions are caused by spontaneous, propagating calcium waves (16). Both their frequency (in the 10-100 mHz range) and amplitude (0-20% diameter reduction) increases as development proceeds (17, 18). We aimed here at understanding how these structural and contractile anisotropies relate to organ growth. To this end, we measured gut passive and active mechanical properties at different developmental stages. We then correlated mechanical properties with the pattern of organ growth in an innovative culture setup. We found that high gut contractility (at E10) was correlated with anisotropic elongational growth in culture whereas low contractility (at E7) resulted in isotropic growth. We further found that inhibiting smooth muscle contractility at E10 by pharmacological or microsurgical methods induced a switch from elongational to radial growth. We conclude that smooth directs the anisotropic growth of the embryonic intestine, and discuss the implications of our findings for mammalian development (mouse, human), short-bowel syndrome and organoid research.

Results

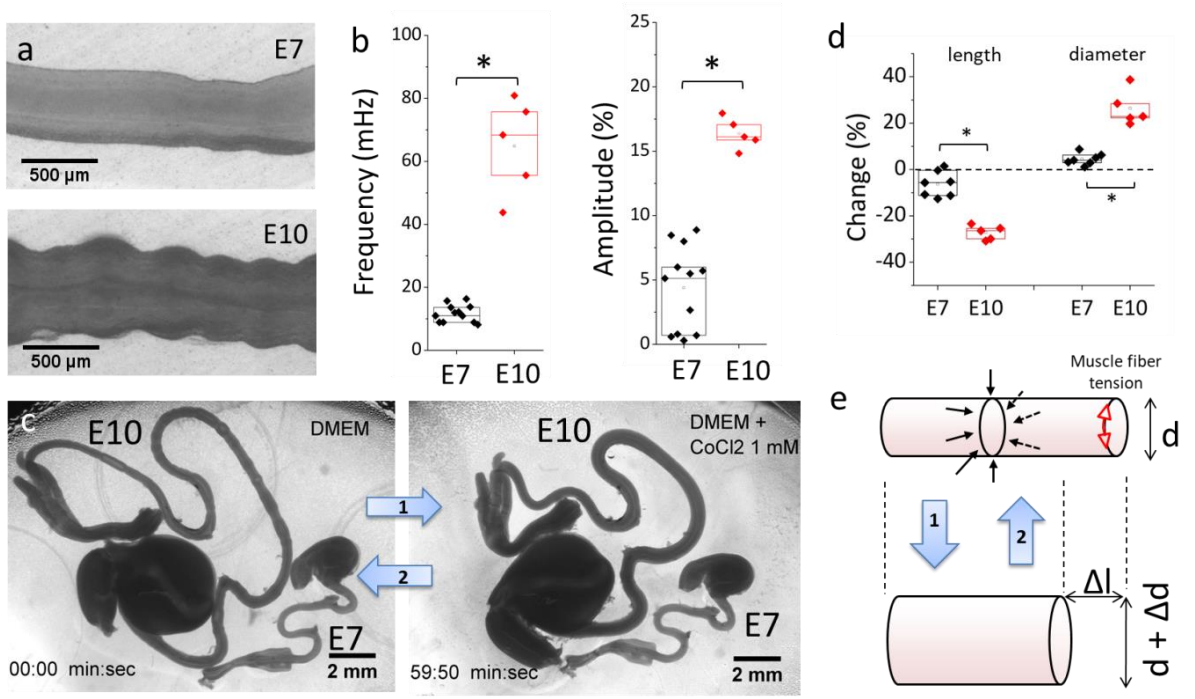

Figure 1. Gut circular smooth muscle (CSM) phasic and tonic properties. (a) Still shots of peristaltic contractions of E7 and E10 guts (VideoS1). (b) Comparison of peristalsis wave frequency and amplitude at E7 (*n*=12) and E10 (*n*=5). All *n* values refer to different guts (different embryos). (c) Still shots of E10 and E7 guts in DMEM at 37°C before and after application of $CoCl_2$ 1 mM for 1 h (Video S2). The drug induces halts spontaneous contractions, as can be seen by comparing the corrugation of the E10 gut before and after application (and in Video S2). It also changes the morphology of the gut. (d) Change in length and diameter of E7 and E10 guts after 1 h $CoCl_2$ application, E7 (*n*=7) and E10 (*n*=5). *p < 0.05, Mann Whitney two-tailed test. (e) Scheme of the deformation induced by circular smooth muscle tone. Muscle fiber tension is indicated with red arrows and the resulting centripetal pressure with black arrows. When CSM fibers contract (arrow 2), gut diameter decreases and the gut elongates.

Circular smooth muscle activation triggers an immediate mechanical elongation of the gut which is significantly more pronounced at E10 than at E7.

E7 and E10 midgut present the same tubular geometry and basic histology: they both have been colonized by enteric neural crest cells (19) and both present a circular smooth muscle ring that gives rise to spontaneous contraction waves (17). Note that the contraction waves are only due to the circular smooth muscle layer, as the longitudinal layer only differentiates at E13 (7) and becomes contractile at E14 (20). We recorded CSM phasic peristaltic activity by time-lapse imaging E7 and E10 guts lying on porous membranes on DMEM at 37°C (Fig.1a, VideoS1, Materials & Methods). The frequency of peristaltic waves at stages E7 (*n*=12) and E10 (*n*=5) was respectively 11.7 ± 2.7 mHz and 64.9 ± 15.2 mHz and their amplitude 4.4 ± 3.3% and 16.4 ± 1.2%. All values in this article are reported as mean ±

standard deviation. Both frequency and amplitude of phasic CSM activity were significantly higher (by a factor ~4-6) at E10 than at E7 (Fig.1a,b). To measure tonic CSM activity, we compared gut morphologies in DMEM at 37°C before and after application of the broad-spectrum calcium channel blocker $CoCl_2$, an efficient inhibitor of CSM activity (17). Within minutes, $CoCl_2$ led to an increase of gut diameter and decrease of gut length (Video S2). After 1h application the shapes of the guts were stable and spontaneous contractions were abolished. Morphological changes were slight at stage E7 but conspicuous at stage E10 (Fig.1c). Length change ε_z at E7 (*n*=7) and E10 (*n*=5) were respectively -6.3 ± 5.5% and -27.2 ± 3.1 %, the accompanying diameter change was respectively 4.5 ± 2.5% and 26.4 ± 7.6%; these differences were statistically significant (Fig.1d). The morphological changes induced by $CoCl_2$ 1 mM applied for 1h are not due to toxicity because these effects were reversible: smooth muscle contractility was recovered (*n*=3) after washing out the drug and incubating E10 guts overnight.

The morphological changes induced by $CoCl_2$ can be explained by a simple mechanical model (Fig.1e): when CSM fibers are active, they contract (red arrowheads), exerting a net uniform, radially oriented pressure on the gut. When CSM tone is relieved by $CoCl_2$ application (arrow 1) the gut increases in diameter and, as a consequence of its incompressibility, shortens (Video S2). Conversely, when CSM contracts (arrow 2), the gut thins out and elongates. Crudely modeling the gut as a cylinder of Poisson ratio $\nu_{\theta z}$ and elastic modulus E_z (see values at E7 and E10 below) an estimate of the pressure generated by smooth muscle $P = E_z\varepsilon_z/\nu_{\theta z}$ can be computed: we find 370 ± 320 Pa at E7 and 1850 ± 370 Pa at E10. The embryonic gut is thus, during development, constantly subject to a centripetal mechanical stress generated by its own musculature, whose net mechanical effect is to cause elongation. We find that this effect is much more pronounced at stage E10 than stage E7, because circular smooth muscle is thicker and stronger at later stages (17).

Both E7 and E10 guts display anisotropic passive mechanical properties

We characterized non-muscle, passive mechanical properties of guts at stage E7 and E10 by performing stretch (Fig.2a) and distension (Fig.2d) assays in DPBS (Ca^{2+} 0.9 mM, Mg^{2+} 0.49 mM) at room temperature. In these conditions, the guts did not exhibit any spontaneous muscle activity, nor was stretching and / or distension able to elicit contractions (16). We used thin, force-calibrated glass cantilevers (Materials & Methods) to measure the longitudinal elastic modulus E_z (Fig.2b,c, Materials & Methods). We found $E_{z,E7}$= 1570 ± 290 (*n*=6) and $E_{z,E10}$= 2460 ± 60 (*n*=6).

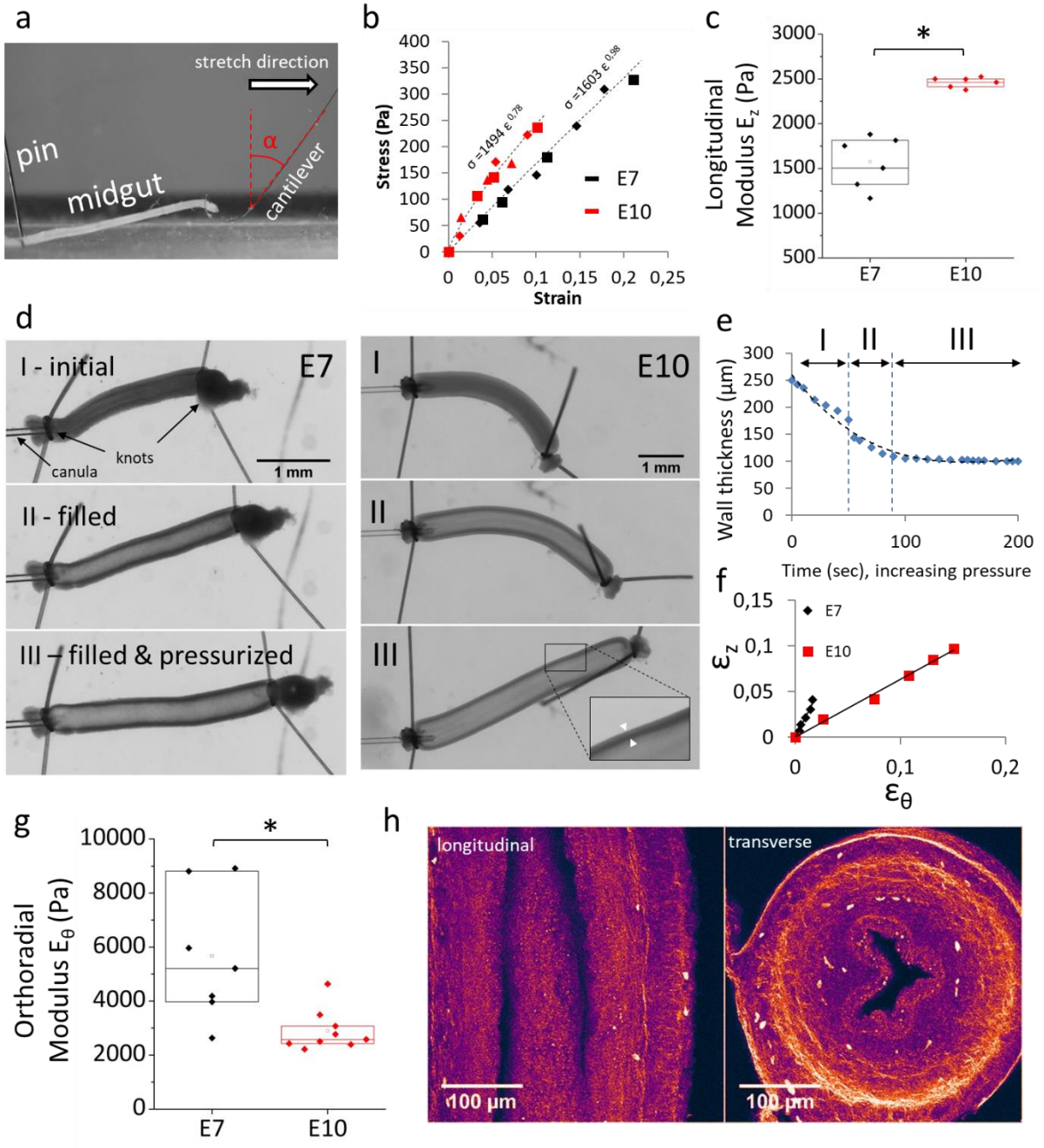

Figure 2. Passive (non-muscle) mechanical properties of the gut. (a) Setup to measure the longitudinal elastic modulus E_Z of the embryonic midgut by stretching with a glass microfiber. (b) Typical stress-strain curves and power law fits (dashed lines). Different symbol shapes correspond to data from consecutives stretches on the same gut (shown here 2 stretches for E7 and *3* stretches for E10). (c) Longitudinal elastic modulus of jejunum at E7 (*n*=6) and E10 (*n*=6). All *n* values refer to different guts (different embryos). (d) Still shots from gut pressurization experiments (VideoS3). Upon pressurization, the gut elongates, increases in diameter and the wall thickness decreases. Inset E10: zoom showing wall-thickness. Note the different scale bars for E7 and E10. (e) Evolution of the wall thickness as a function of time (here at E10), dashed line: polynomial fit. (f) Representative diameter change ε_θ versus length change ε_z at E7 and E10. (g) Orthoradial elastic modulus E_θ at E7 (*n*=7) and E10 (*n*=9), phase II. (h) Second harmonic generation (SHG) images of longitudinal (left) and transverse (right) sections of E9 jejunum. Collagen I&III are the main molecules contributing to the SHG signal. *p < 0.05, Mann Whitney two-tailed test.

To measure the orthoradial elastic modulus E_θ, we canulated a midgut segment with a micropipette, sealed the segment and monitored thickening ε_θ, lengthening ε_z and wall-thickness w as fluid pressure in the gut lumen was increased (Video S3, Fig.2d). In the initial stages of pressurization, the gut wall thins out significantly as the lumen gets filled with fluid (Fig.2d&e, I); as pressure is further increased, the change in wall thickness becomes small (Fig.2d&e, II) and even negligible (Fig.2d&e, III). In phases II&III the gut can be modeled as an orthotropic, thin-walled cylinder with anisotropic mechanical properties along two axes. The ratio of lengthening over thickening $\varepsilon_z/\varepsilon_\theta$ during phase II of the inflation (Fig.2f) at stages E7 and E10 were respectively 2.4 ± 0.3 and 1.1 ± 0.8, yielding $E_{\theta,E7} = 7730$ ± 890 Pa and $E_{\theta,E10} = 5340$ ± 310 Pa (Fig.2g&S1, Materials & Methods). For an isotropic pressurized cylindrical shell has $\varepsilon_z/\varepsilon_\theta$ = 0.5. From the values of $\varepsilon_z/\varepsilon_\theta$ measured above, we can conclude that both E7 and E10 guts are anisotropic. We found similar results analyzing phase III data (Fig.S2). Second harmonic generation imaging (SHG, cf Materials & Methods) shows that collagen fibers (15) form a dense circumferential ring (Fig.2h, right), whereas longitudinal fibers are scarce (Fig2h, left). This molecular-scale anisotropic structure is consistent with the macro-scale stiffness anisotropy we report.

In culture, E7 guts grow isotropically whereas E10 guts elongate anisotropically

We next examined how muscle and non-muscle mechanical properties relate to growth of the organ. We have previously demonstrated that, *in-ovo*, the gut loop is stretched by the vitelline duct (12). To isolate the effect of smooth muscle force on growth we therefore dissected the guts from their surrounding tissues. We found that an appropriate oxygen supply was critical to achieve growth of the isolated intestine. By constantly bubbling carbogen (95% O_2 – 5% CO_2) in the culture medium (Fig.3a), we established an oxygen level of 24.2 mL/L in the vicinity of the guts that is in the range of oxygen levels measured in the chorioallantoic vein of chicken embryos at similar stages (see Materials & Methods). Video S4 shows the vivid peristaltic activity of E10 guts after 48h culture in these conditions. Immediately after removing samples from culture, guts appeared very elongated because of CSM activity (see mechanism in Fig.1e). After 1h in DPBS at room temperature, CSM activity became extinct and the guts had relaxed to a stationary shape. In these conditions, the shape of the guts after culture could be compared in the same physico-chemical conditions (DPBS at RT) as before culture (i.e., after dissection). Fig.3b shows representative morphological changes of E7 and E10 midguts (duodenum to ileum) before and after culture. We quantitatively assessed these morphological changes using a Voronoi algorithm (Materials & Methods). We found that gut length, diameter and volume increased respectively by 12 ± 21%, 33 ± 12%, 94 ± 34% at stage E7 (n=15) and 25 ± 14%, 7 ± 7%, 44 ± 20% at stage E10 (n=32).

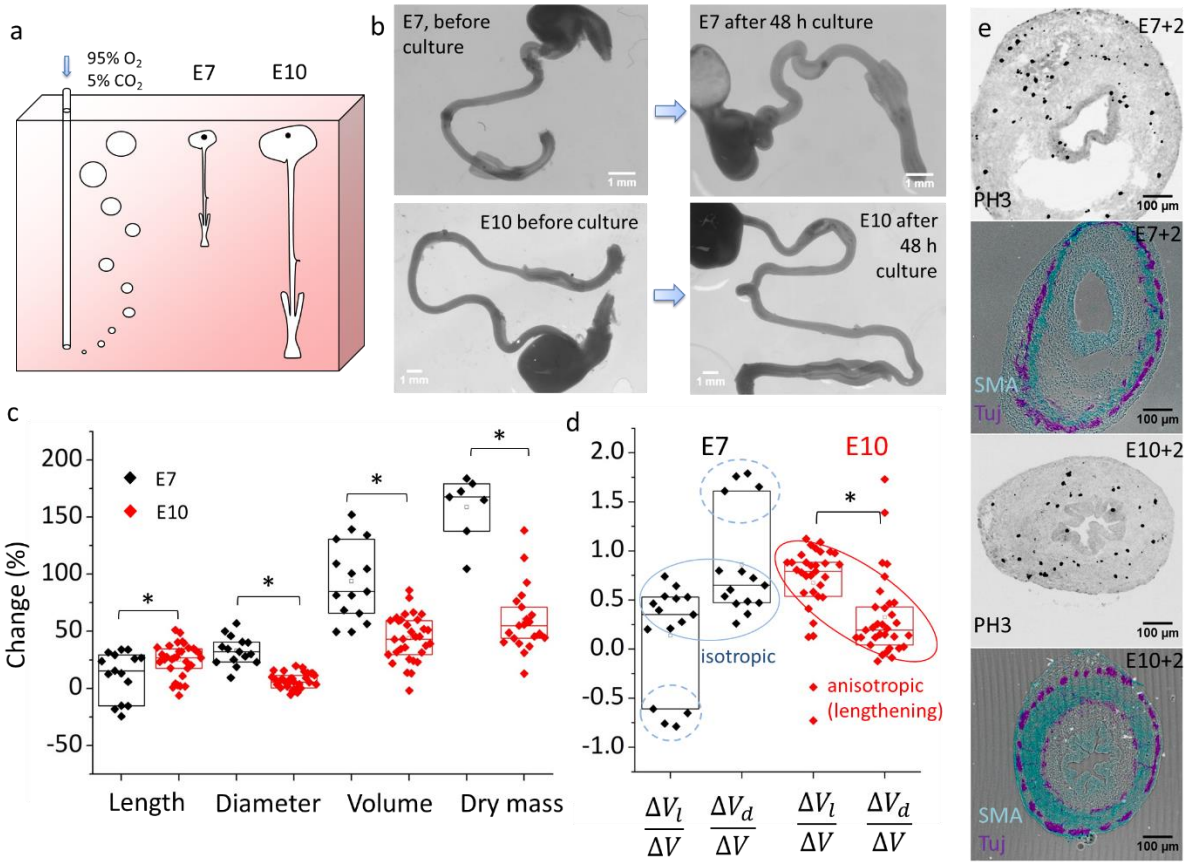

Figure 3. Compared growth pattern of E7 and E10 guts in culture. (a) Scheme of the culture system (Materials and Methods). (b) Representative images of E7 and E10 guts before and after 48h culture and subsequent relaxation of the guts for 1h in PBS. (c) Length, diameter, volume and dry mass change of E7 (*n*=15) and E10 (*n*=32) guts after 2 day culture and 1h relaxation in PBS. Each *n*-value and data point corresponds to a different gut (different embryo). (d) Relative contributions of lengthening $\Delta V_l/\Delta V$ and thickening $\Delta V_d/\Delta V$ to growth at stage E7 and E10. Note that $\Delta V_l/\Delta V$ and $\Delta V_d/\Delta V$ for each sample are related by $\Delta V_l/\Delta V + \Delta V_d/\Delta V = 1$, i.e., the data has a mirror symmetry around the horizontal axis corresponding to isotropic growth $\Delta V_l/\Delta V = \Delta V_d/\Delta V = 0.5$. (e) Immunohistochemistry for proliferating cells (anti-histone H3 phospho S10), smooth muscle α-actin (SMC, red) and βIII-tubulin (green, enteric neurons) on E7 and E10 transverse sections after 2 day culture. *p < 0.05, Mann Whitney two-tailed test.

Length increase was higher at E10 than at E7, while diameter and overall volume increase was higher at E7 than at E10; all differences were statistically significant (Fig.3c). Culture led to a dry mass increase (Materials & Methods) of 159 ± 28% at stage E7 (*n*=7) and 60 ± 29% at stage E10 (*n*=21). The ~3 times higher volume and dry mass growth rate of E7 guts compared to E10 could be due to the higher proportion of proliferative, non-differentiated cells at younger stages or to the better oxygen tissue perfusion of the smaller E7 guts. Fig. 3e shows that proliferating, histone 3 (phospho S10)-positive cells were found throughout the gut mesenchyme and epithelium after culture. Guts featured well defined enteric and smooth muscle layers (Fig. 3e, Tuj&SMA). The CSM ring was much thicker for E10+2 than for E7+2 guts. To quantify growth anisotropy, we computed the contributions of lengthening ΔV_l and thickening ΔV_d (Materials & Methods) to the overall volume change ΔV. We found that most (*n*=11/15) E7 guts grew isotropically (i.e. $\Delta V_l/\Delta V \sim \Delta V_d/\Delta V \sim 0.5$, Fig.3d, blue circle); some samples (*n*=4/15) thickened and shortened (Fig.3d, dashed blue circle). In contrast, E10 guts anisotropically lengthened (Fig.3d, red circle) in 80% of samples (*n*=26/32). The remaining 20 % of samples (*n*=6/32) thickened

rather than lengthened. We found that out-of-trend behaviors in both age groups were correlated with low overall growth (Fig.S3), indicating that they may result from poor vitality of the organ after dissection or during culture.

We visualized the elongational growth of E10 guts in culture by time-lapse imaging (Video S5): the guts are initially pinned at their extremities and buckle as they progressively elongate, while undergoing constant peristaltic wave activity. This is to our knowledge the first live, organ-scale video of a growing embryonic gut.

Inhibition of smooth muscle contractions by pharmacological or surgical means induces a switch from elongational to radial growth

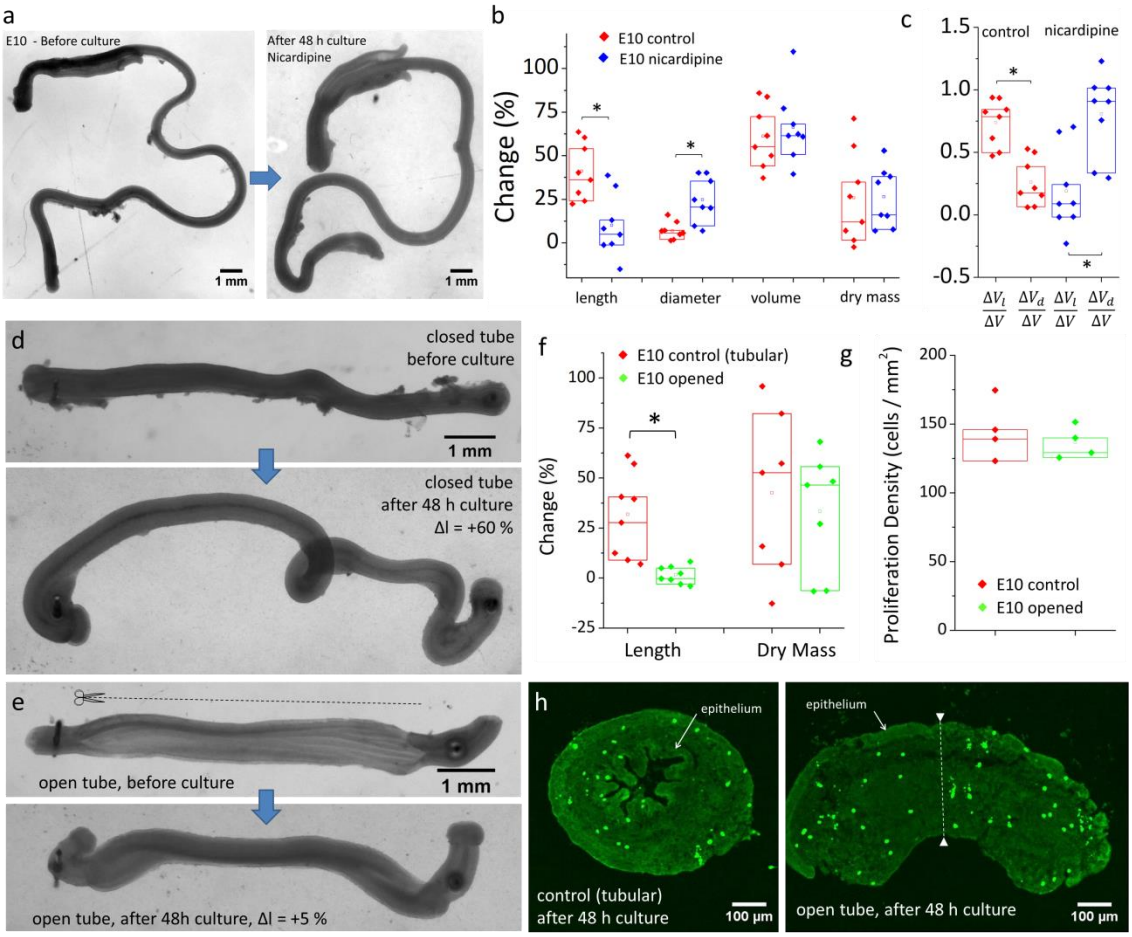

Figure 4. Disrupting smooth muscle contractions pharmacologically (a-c) or surgically (d-h) induces a switch from elongational to radial growth. (a) Example image of E10 gut cultured with L-type channel blocker nicardipine (5 µM) before and after culture. The gut thickened but length change was small. (b) Length, diameter, volume, dry mass change and (c) growth anisotropy of control (*n*=8) and nicardipine treated (*n*=8) guts after 2 day culture. Each n-value and data point corresponds to a different gut (different embryo). (d) Closed (control) and opened (e) E10 gut segments after 48 h culture, Δl indicates the length change. The cut was performed longitudinally, along one border of the gut (dashed line), causing the gut to spring open, revealing the epithelial grooves inside. (f) Length and dry mass change of control (*n*=8) and opened (*n*=8) segments. (g) Density of proliferating (PH3-positive) cells of closed (*n*=4) and opened (*n* = 4) gut segments, assessed from (h) confocal images of anti-histone H3 phospho S10 immunolabeled transverse gut sections after 48 h culture. *p < 0.05, Mann Whitney two-tailed test.

Weakly contractile E7 guts grow isotropically whereas strongly contractile E10 guts grow anisotropically (Fig.1&Fig.3). To investigate the possibility that contractility be causal in directing growth anisotropy, we pharmacologically inhibited smooth muscle contractions with the L-type calcium channel inhibitor nicardipine (21). This dihydropyridine derivative has been shown to inhibit contractility in the embryonic mouse gut (18) and is used for the treatment of hypertension and angina pectoris (22). It was therefore a promising candidate to relax muscle activity without affecting tissue viability and growth. We found that 5 µM nicardipine consistently abolished motility in the whole gut within 10 min after application. Whereas motility in the caeca and hindgut was abolished for 48 hours following application, motility in the midgut gradually recovered, albeit at a much reduced amplitude and frequency compared to control guts (Fig.S4a,b). The volume and mass increase of control and nicardipine-treated guts were similar (Fig.4b) after 48 h culture. However, whereas control guts featured anisotropic longitudinal growth (Δl =42±16 %, Δd=7±5 %, *n*=8 Fig.4b-c), nicardipine-treated guts grew mostly radially (Δl =12±17 %, Δd=24±13 %, *n*=8, Fig.4a-c).

As a further test of the muscle-driven anisotropic growth theory, we disrupted the continuity of the line of tension generated by circular smooth muscle by cutting longitudinally one gut wall with surgical micro-scissors (Fig.4e). When the gut wall is cut, circumferential tension is released, causing the gut to open up and become a ~2D sheet of tissue. This procedure has been used to measure circumferential stress in arteries (23) and prepare 2D gut tissue for physiology (24) and developmental biology (25) experiments. We compared the growth characteristics after 48 h of intact (tubular) gut segments (Fig.4d) with those of opened segments (Fig.4e). We found that the length change (Fig.4f) of the tubular and opened segments were respectively 27 ± 21 % (*n*=8) and 1.7 ± 4.4% (*n*=8), i.e., tubular segments elongated whereas open segments did not. Open segments after 48 h were characterized by an exteriorized epithelium that covered the outer periphery of the explant (Fig.4h). Although we could not directly quantify their diameter and volume from 2D pictures, transverse sectioning revealed that the opened segments after culture (Fig.4h right) were noticeably and uniformly thicker (dashed white line) than one wall (i.e., the radius) of the closed tubes (Fig.4h left). We investigated whether surgical opening of the segments could have induced growth defects by intrinsically reducing explant viability or proliferation. We found that all opened explants (*n*=8) still displayed rhythmic smooth muscle contractions after 48 h culture, albeit not leading to elongation as described in Fig.1e. We found that the dry mass increase of samples (Fig.4f) and the density of proliferating cells (Fig.4g) after 48 h culture were similar for tubular and opened preparations. This indicates that the elongation defect in opened preparations is due to the inhibited self-squeezing effect (Fig.1e) following disruption of the circumferential tension generated by the circular smooth muscle.

Discussion

Together, the embryological (E7 vs E10, Fig.3), pharmacological (nicardipine inhibited contractions at E10, Fig.4a-c) and microsurgical (opened E10 segments, Fig.4d-h) comparative growth experiments all indicate that anisotropic elongational growth is severely affected when circular smooth muscle contractions are weak or otherwise disrupted. These results show that the short-time scale (~1h), purely mechanical lengthening induced by CSM contractions we described in Fig.1c-e leads to irreversible elongational growth when these deformations are cumulated on long time scales (48h), as first hypothesized in 1952 by Coulombre & Coulombre (26).

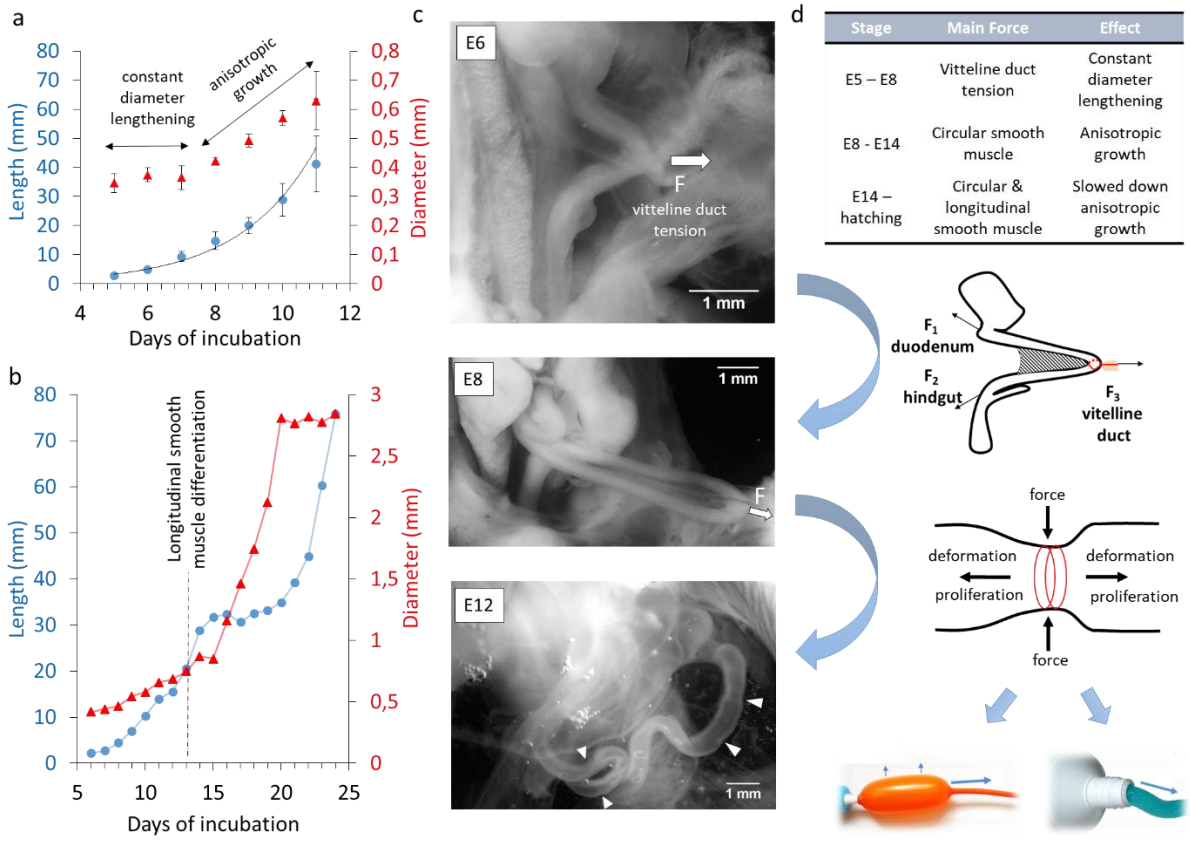

Figure 5. Growth kinetics and mechanical forces acting on the gut during embryogenesis. (a) Physiological evolution of chicken midgut length (blue circles) and average diameter (red triangles). The midgut comprises the duodenum, jejunum and ileum up to caecal appendix tips. Sample numbers: E5 *n*=8, E6 *n*=7, E7 *n*=5, E8 *n*=6, E9 *n*=7, E10 *n*=8, E11 *n*=7. Error bars are ±SD. The length is fitted with an exponential (black line). The growth curves are consistent with those reported by other investigators (26, 27). **(b) Length (blue circles) and diameter (red triangles) evolution of the duodenum from E6 to 3 days post-hatching, each point is the mean of at least 10 specimens. The experimental data was collected by Coulombre & Coulombre** (26) **and is adapted here. (c) Representative pictures of E6, E8 and E12 guts in the abdominal cavity of the embryo in PBS, immediately after it was extracted from the egg. The pulling force *F* exerted by the vitelline duct at stage E6 and E8 is indicated with an arrow. At stage E12, spontaneous *in vivo* CSM contractions are conspicuous (white arrowheads). (d) Proposed model of the main forces acting on the embryonic gut at different developmental stages and of their relation to organ growth. Bottom images: inflation of an anisotropic**

balloon or squeezing of a tube of toothpaste illustrate two possible mechanisms by which circular mechanical constraints can lead to anisotropic deformation or flow.

Different mechanical forces guide the growth of the developing intestine

Importantly, although E7 guts presented anisotropic non-muscle mechanical properties (Fig.2c,g), they grew isotropically in culture (Fig.3d). This shows that the information leading to anisotropic gut growth is not encoded 1°) by molecular information contained within individual cells of the gut, 2°) by the initial cylindrical geometry of the gut or 3°) by passive, non-muscle tissue mechanical anisotropies (i.e., collagen fiber orientation). We have recently shown (12) that, from E5 to ~E9, a tensile force transmitted via the vitelline duct pulls the early gut loop out of the coelom (white arrow in Fig.5b, free-body diagram in Fig.5c), causing physiological herniation. We had demonstrated (12) that applying a static, longitudinally-directed force mimicking the vitteline duct tension to E7.5-E8 guts in culture was sufficient to induce anisotropic elongational growth. Here we find that E7 guts not subject to an externally applied mechanical force grow isotropically when perfused with O_2. Together, these experimental facts support the view that the tensile force transmitted via the vitelline duct is essential for the initial physiological constant-diameter lengthening (Fig.5a) of the gut. This umbilical pull sets the initial high aspect ratio of the organ.

As from ~E10, vitteline duct tension becomes negligible as additional gut loops start forming by buckling (28) (Fig.5b, E12). The dominant mechanical constraint acting on the gut as from this stage (Fig.5a, phase B) are compressive, radially oriented forces due to CSM contractions (Fig.5b&c, E12, *in-vivo* phasic contractions are pointed at with white arrowheads). We have demonstrated here that CSM forces alone can drive further anisotropic growth. CSM could act as a stiff corset (8) that skews proliferation along the longitudinal direction (Fig.5c, anisotropic balloon analogy). Phasic contractions could also make the tissue creep in the longitudinal direction (Fig.5c, toothpaste analogy), by actively remodeling cell-cell and cell-matrix junctions in the gut interior. Longitudinal smooth muscle differentiates in the chicken at E13 (7). Our mechanical growth model correctly predicts that the buildup of tone and phasic contractions along the longitudinal direction shortly thereafter, at E14 (20), initiates a period of relatively slower longitudinal growth and relatively faster diameter growth (Fig.4b, experimental data adapted from Coulombre et al. (26)).

The functional role of contractile waves generated by spontaneous calcium transients (16–18) in the developing gut has remained obscure, because the digestive tract does not transport any nutrients during embryogenesis. Our results show that these waves, together with smooth muscle tone, drive intestinal elongation. This provides a striking example of how the mechanical function of an organ (peristalsis) drives its shape (morphogenesis).

Mouse smooth muscle mutants exhibit growth defects.

Several groups have reported gut morphological phenotypes in mice with genetically disrupted smooth muscle. Mutations included LMOD1(29), laminin α5(30), and Brahma (Brm) & Brahma-related gene 1 (Brg1)(31). In all of these studies, weakened smooth muscle contractility, differentiation or organization resulted in significantly shorter (50-80% wildtype length), bulkier guts at embryonic stages. These findings support the role of smooth muscle as an essential driver of gut elongation in the embryo. Care must however be taken in comparing the morphogenesis in different animal species. Whereas epithelial villi formation in the chicken results from a mechanobiological buckling instability (7), their emergence in mice is independent from muscle activity and can be derived from a Turing field in which an inhibitor of Bmp signaling acts as the Turing activator (25). It cannot therefore be excluded that mechano-biologically driven scenarios of organogenesis in the avian embryo may differ in mammals.

Implications for human gut development, short-bowel syndrome and organoids

As a rule of thumb, days of development in the chicken correspond to weeks of development in the human (20). In the human embryo, MRI imaging of the gut of embryos from the Kyoto collection (32) show it forming a hairpin-like umbilical hernia between Carneggie stages (CS) 14 and 18 (week 5-7), much like in the early chicken embryo (Fig.5b, E8). Distinct undulations of the gut are seen at stages CS19-CS21 (week 7.5-8), that are similar to the phasic smooth muscle activity seen in the chicken in Fig.1a. Although not commented upon by the authors (32), these undulations are, to the best of our knowledge, the first evidence of early gut motility in the human embryo. We believe that contractions of the gut can be seen because the embryos of the Kyoto collection were immediately fixed in paraformaldehyde following abortion. The presence of contraction waves at this stage is consistent with the fact that CSM is differentiated (33) in the human gut at least as from CS 18 (week 7). Vitelline duct tension and the squeezing effect due to CSM are thus present at early embryonic stages in the human embryo as well, raising the possibility that the mechanically-driven growth mechanism we demonstrated in the chicken (Fig.5) may also apply to humans. Short Bowel Syndrome (SBS) is a devastating pathology resulting in dramatically reduced gut growth. Mutations in *CLMP* and *FLNA* have recently been found to cause SBS (34). FLNA binds to actin and CLMP co-localizes with actin filaments. CLMP has moreover been found to strongly downregulate the expression of connexin 43 and 45 in mice (35), and we have recently shown that gap junctions (connexins) are essential for early gut motility (16). Both actin-binding protein and connexin defects could severely hamper normal CSM contractility, relating it to the SBS phenotype. This causal link remains to be asserted however, because it is unclear whether SBS is paired with defective gut contractility or motility (34). Mechanical distension is being considered to lengthen the intestine of SBS patients (36). Our research suggests that an innovative therapeutic approach could involve boosting motility and circular smooth muscle tone.

Intestinal stem-cell derived organoids can adopt star-like shapes (2). We believe that this may be due to a mechano-biological growth instability: if the initially spherical shell of smooth muscle within the organoid develops more in some locations than in others, these spots will experience greater smooth muscle strain, elongate, thus giving rise to protrusions (the arms of the star). Just like asymmetric chemical signaling cues (37), mechanical forces can provide a symmetry-breaking cue. Our study suggests that a way of growing anisotropic, cylindrical organoids would require breaking the initial spherical symmetry of the system, e.g. by depositing the stem cells on a rectangular pattern or in a cylinder. Our investigations reinforce the view that smooth-muscle generated forces (8, 9) play a central role in establishing whole-organ shape, and thus functionality. Controlling the geometry and direction of contraction forces generated by muscle within organoids will prove essential for tissue engineering and for the interpretation and remediation of organ growth defects.

Materials and Methods

Specimen preparation

Fertilized chicken eggs were purchased from EARL Morizeau (Chartres, France, breeder Hubbard, JA57 hen, I66 rooster, yielding type 657 chicks). The eggs were incubated at 37.5°C in a humidified chamber for 5 to 12 days. The gastrointestinal tract was dissected out from the embryos from hindgut to proventrilicus and the mesentery carefully removed.

Characterization of smooth muscle contractility & passive mechanical properties

To characterize their peristaltic activity, guts at stage E7 and E10 were placed on Anodisc membranes (Whatman, pore size 0.2 µm) resting on cylindrical wells filled with DMEM GlutaMAX™-I (with 4.5 g/L D-glucose and sodium pyruvate), as previously described(17) . To characterize static CSM tone, freshly dissected guts were incubated at 37°C in a 5% CO_2 atmosphere for 1 h in a thin (0.5 mm) layer of DMEM. In this configuration the whole gut is free to move and deform, whereas meniscus forces hold the gut down on Anodisc membranes. 1 mM of $CoCl_2$ was introduced and the morphological changes of the guts were monitored after ~1h (at which time they had reached a stationary state, cf VideoS2). We characterized motility by computing the speed of the waves and their frequency $f = n/\Delta t$, where n is the number of waves passing through a given position in a time Δt. The amplitude was measured directly from the video as $A = (d_{rest} - d_{constricted})/d_{rest}$, where d_{rest} is the resting diameter of a point along the gut and $d_{constricted}$ is the diameter at the same position when it is constricted by a contraction wave. Characterization of passive mechanical properties relies on previously established protocols (38) and microscopy techniques (15) that we describe in the Supplementary Information.

Organotypic culture

For E7-E10 compared growth (Fig.3), the stomach of demesenterized guts was pinned with a needle to the side of a Sylgard coated rectangular trough (H x W x D 50x80x32 mm) filled with 140 mL DMEM supplemented with 1% penicillin-streptomycin. The medium was saturated with carbogen (95% O_2, 5% CO_2) by continuous bubbling. For reference, blood in the vitteline artery (supplying the gut) in the chicken embryo at E6 has a total oxygen concentration (dissolved + carried by hemoglobin) of 13.5 mL/L(39), and of 89 mL/L(40) in the blood of the chorioallantoic vein at E10. The equilibrium dissolved O_2 concentration of carbogen at 37.5°C is 24.2 mL/L, which lies in this physiological range. We verified this value (Fig.S5a) by direct measurement with a Clark-type electrode (Unisense, Denmark). We set the carbogen bubbling rate so that rising bubbles generated a light convection current in the trough. This insured that oxygen was replenished in the vicinity of the guts, without exerting significant hydrodynamic forces on the guts. The density of the guts is almost that of the culture medium, so that gravity effects can be neglected. In this culture system, the only forces acting on the guts are the phasic and tonic components of the smooth muscle. The trough was covered with a cap and the guts cultured for 2 days in a humidified incubator (Thermos) at 37.5°C. For the experiments with nicardipine (Fig.4a-c), gut growth was achieved by putting individual samples in a shallow layer of medium (1 mL in a 35 mm diameter Petri dish) and incubating all samples in an atmosphere of 95% O_2, 5% CO_2 at 37°C. Diffusion of the oxygen through the shallow layer of DMEM resulted in a concentration of 21±5 mL/L O_2 (n=3) at a distance of ~1 cm from the organ (measured with Clark electrode, see Fig.S5b). Nicardipine was prepared as a stock solution (10 mM) in DMSO and diluted in the medium to 5 µM. Control guts were incubated in the equivalent quantity of vehicle, i.e. 0.5 ‰ DMSO. Drug and medium were refreshed after 24h culture. For open gut preparations (Fig.4d-h), ~1 cm long E10 gut segments were pinned at one end to a Sylgard-covered tray. The opening was performed with Vannas microscissor (CM-85-AS30, Euronexia, France) and with the help of a binocular. Samples were then pinned to the other end and cultured in a shallow layer of DMEM (1 mL in a 35 mm diameter Petri dish) in a carbogen atmosphere for 48 h. Morphology of all guts pre-culture was measured in DBPS at room temperature. Morphologies of all guts post-culture (Fig.3,4) was measured after relaxation of the samples for 1 h in DBPS at room temperature.

Analysis of gut morphometric changes

We follow a procedure previously described (12). Raw images of the guts lying in a shallow depth of DPBS (so they were in 2D plane) were processed to erase the hindgut, stomach and any residual tissue around the axially-symmetric midgut (segment comprised between caecal appendix tip to duodenum-stomach junction). We then thresholded these images and extracted the midgut contour (Matlab routine). We next applied a Voronoi Matlab algorithm to this contour to obtain the gut midline length, average diameter, and volume. We neglect the volume occupied by the lumen, which is close to 0 at E7, and

only ~5% at E10 (7). In ~20% of samples after culture, certain regions of the guts presented local (along max ~10% of gut length) accumulation of intraluminal fluid or DMEM – we erased these bulges to exclude them from the total volume. Lengthening ΔV_l and thickening ΔV_d were defined as $\Delta V = \Delta V_l + \Delta V_d = \frac{\partial V}{\partial l}\Delta l + \frac{\partial V}{\partial d}\Delta d = \pi d^2 \Delta l/4 + \pi d l \Delta d/2$, where ΔV is the total volume change, d and l are respectively the initial gut average diameter and length and Δd and Δl the gut diameter and length change induced by culture. Isotropic growth corresponds to $\Delta V_l/\Delta V = \Delta V_d/\Delta V = 0.5$.

Dry mass determination

Water was removed from the midguts by bathing them successively in 1:2, 2:1 and 1:0 absolute ethanol:water mixtures, for 30 minutes in each solution. This procedure warrants that all ethanol-miscible components like water, salts and any residual intraluminal fluid are washed away. Guts were then dried in air either on steel pins or on a weighing cantilever (E7). Dry masses of native and cultured E10 guts were measured with a precision balance (Sartorius). For E7 guts, the balance did not provide the required precision, we weighed them using calibrated cantilevers as previously described (12). We measured a dry mass density of native E7 and E10 guts of ρ_{E7} = 0.097 ± 0.01 mg/mm^3 (n = 4) and ρ_{E10} = 0.125 ± 0.002 mg/mm^3 (n =7). We used these densities to compute the initial dry mass m_i of the guts before culture, $m_i = \rho_{E7\ or\ E10} V_i$, where V_i is the initial volume. The dry mass change induced by culture (Fig.3c, Fig.4b,f) is $(m_f - m_i)/m_i$, where m_f is the measured dry mass of the gut after culture.

Immunohistochemistry

Guts were fixed for 1 h in a 4% PFA in PBS solution, washed in PBS, then let overnight in 30% sucrose in water solutions, and embedded the next day in OCT compound (VWR) on dry ice. Thin (14 µm) slices were cut at -20°C in a Leica cryotome and deposited on Thermofrost glass slides. After rehydration, the slides were blocked for 15 min in a 1% BSA and 0.1% triton in PBS solution, the slides were then incubated overnight in anti-α smooth muscle actin antibody (Abcam, ref5694, dilution 1:2000), anti βIII-tubulin antibody (Abcam, ref14545, dilution 1:1000) or anti-Histone H3 (phospho S10) (Abcam, ref14955, dilution 1:200) solution composed of 1% BSA in PBS; the following day, after washing, CY3- and A488-conjugated secondary antibodies (ThermoFisher, dilution 1:400 in PBS) were applied for 2 h. The slides were washed in PBS, and immediately imaged in a layer of PBS with a confocal microscope (Olympus).

Acknowledgments. We thank Etienne Couturier for help interpreting inflation experiments, Vincent Fleury for stimulating discussions and Alexis Peaucelle for proofreading the manuscript. **Funding.** This research was funded by a CNRS / INSIS Starting Grant “Jeune Chercheur” and by the CNRS "Défi Mécanobiologie 2018". The authors acknowledge Thomas Guilbert from IMAG’IC for assistance with SHG Imaging. **Author Contributions.** DK, YK, ND, NRC performed experiments and analyzed data; NRC conceptualized and supervised the research and wrote the article. **Competing Interests.** The

authors have no competing interests **Ethics Statement.** The experiments were conducted under European law article 2016/63/UE. The approval of experimental protocols by an ethics committee is not required for research conducted on chicken at embryonic stages. All experiments were performed in accordance with the ethics guidelines of the INSERM and CNRS. **Statistical analysis.** All samples are included in the presented data, no randomization or blinding was used, median, upper (75%) and lower (25%) interquartile range and means (empty square) are presented in Fig.1-5. All pairwise statistical analysis were performed using a two-tailed Mann-Whitney test. Differences were considered statistically meaningful at $p < 0.05$ (indicated by a star). **Data availability.** All data are presented in the manuscript.

References

1. Workman MJ, et al. (2016) Engineered human pluripotent-stem-cell-derived intestinal tissues with a functional enteric nervous system. *Nat Med* 23(1):49–59.

2. Fatehullah A, Appleton PL, Näthke IS (2013) Cell and tissue polarity in the intestinal tract during tumourigenesis: Cells still know the right way up, but tissue organization is lost. *Philos Trans R Soc B Biol Sci* 368(1629). doi:10.1098/rstb.2013.0014.

3. Poling HM, et al. (2018) Mechanically induced development and maturation of human intestinal organoids in vivo. *Nat Biomed Eng*:1.

4. Felsenthal N, Zelzer E (2017) Mechanical regulation of musculoskeletal system development. *Development* 144(23):4271–4283.

5. Nelson CM, et al. (2017) Microfluidic chest cavities reveal that transmural pressure controls the rate of lung development. *Development* 144(23):4328–4335.

6. Hilton W (1902) The morphology and development of intestinal folds and villi in vertebrates. *Am J Anat* 1(4):459.

7. Shyer AE, et al. (2013) Villification: how the gut gets its villi. *Science* 342(August):212–8.

8. Jaslove JM, Nelson CM, Nelson CM (2018) Smooth muscle : a stiff sculptor of epithelial shapes.

9. Huycke TR, Tabin CJ (2018) Chick midgut morphogenesis. *Int J Dev Biol* 62(1–3):105–115.

10. Koyama H, et al. (2016) Mechanical Regulation of Three-Dimensional Epithelial Fold Pattern Formation in the Mouse Oviduct. *Biophys J*. doi:10.1016/j.bpj.2016.06.032.

11. Vuong-Brender TTK, Ben Amar M, Pontabry J, Labouesse M (2017) The interplay of stiffness and force anisotropies drives embryo elongation. *Elife*. doi:10.7554/eLife.23866.

12. Chevalier NR, et al. (2018) Mechanical Tension Drives Elongational Growth of the Embryonic Gut. *Sci Rep* 8(1):1–10.

13. Safford SD, Freemerman a J, Safford KM, Bentley R, Skinner M a (2005) Longitudinal mechanical tension induces growth in the small bowel of juvenile rats. *Gut* 54:1085–1090.

14. Beaulieu J, Jutras S, Durand J, Vachon PH, Perreault N (1993) Relationship between tenascin and t-smooth muscle actin expression in the developing human small intestinal mucosa. *Anat Embryol*:149–158.

15. Chevalier NR, et al. (2016) How tissue mechanical properties affect enteric neural crest cell migration. *Sci Rep* 6:20927.

16. Chevalier NR (2018) The first digestive movements in the embryo are mediated by mechanosensitive smooth muscle calcium waves. *Philos Trans R Soc B Biol Sci* 373:1759.

17. Chevalier NR, Fleury V, Dufour S, Proux-Gillardeaux V, Asnacios A (2017) Emergence and development of gut motility in the chicken embryo. *PLoS One* 12(2):e0172511.

18. Roberts RR, et al. (2010) The first intestinal motility patterns in fetal mice are not mediated by neurons or interstitial cells of Cajal. *J Physiol* 588(7):1153–1169.

19. Nagy N, Goldstein AM (2017) Enteric nervous system development: A crest cell's journey from neural tube to colon. *Semin Cell Dev Biol*. doi:10.1016/j.semcdb.2017.01.006.

20. Chevalier N, et al. (2019) Embryogenesis of the Peristaltic Reflex. *J Physiol* 597(10):2785.

21. Bayguinov O, Hennig GW, Sanders KM (2011) Movement based artifacts may contaminate extracellular electrical recordings from GI muscles. *Neurogastroenterol Motil*. doi:10.1111/j.1365-2982.2011.01784.x.

22. Opie LH (2012) Pharmacological differences between calcium antagonists. *Eur Heart J* 18:A71–A79.

23. Fung YC, Liu SQ (1989) Change of residual strains in arteries due to hypertrophy caused by aortic constriction. *Circ Res*. doi:10.1161/01.RES.65.5.1340.

24. Hennig GW, et al. (2010) ICC-MY coordinate smooth muscle electrical and mechanical activity in the murine small intestine. *Neurogastroenterol Motil* 22(5):1–20.

25. Walton KD, et al. (2016) Villification in the mouse: Bmp signals control intestinal villus patterning. *Development* 143(3):427–436.

26. Coulombres A, Coulombres J (1958) Intestinal Development: Morphogenesis of the Villi and Musculature. *J Embryol Exp Morph* 3(3):403–411.

27. Binder BJ, Landman KA, Simpson MJ, Mariani M, Newgreen DF (2008) Modeling proliferative tissue growth: A general approach and an avian case study. *Phys Rev E - Stat Nonlinear, Soft Matter Phys* 78(3). doi:10.1103/PhysRevE.78.031912.

28. Savin T, et al. (2011) On the growth and form of the gut. *Nature* 476:57–62.

29. Halim D, et al. (2017) Loss of LMOD1 impairs smooth muscle cytocontractility and causes megacystis microcolon intestinal hypoperistalsis syndrome in humans and mice. *Proc Natl Acad Sci* 114(13):E2739–E2747.

30. Bolcato-Bellemin AL, et al. (2003) Laminin α5 chain is required for intestinal smooth muscle development. *Dev Biol* 260(2):376–390.

31. Zhang M, et al. (2011) SWI/SNF Complexes Containing Brahma or Brahma-Related Gene 1 Play Distinct Roles in Smooth Muscle Development. *Mol Cell Biol* 31(13):2618–2631.

32. Ueda Y, Yamada S, Uwabe C, Kose K, Takakuwa T (2016) Intestinal Rotation and Physiological Umbilical Herniation During the Embryonic Period. *Anat Rec* 299(2):197–206.

33. Romanska H, Moscoso G, Polak H, Draeger A (1996) Smooth muscle differentiation during human intestinal development. *Eur J Transl Myol* 6(1):13–19.

34. van der Werf CS, Halim D, Verheij JBGM, Alves MM, Hofstra RMW (2015) Congenital Short Bowel Syndrome: from clinical and genetic diagnosis to the molecular mechanisms involved in intestinal elongation. *Biochim Biophys Acta - Mol Basis Dis* 1852(11):2352–2361.

35. Langhorst H, et al. (2018) The IgCAM CLMP regulates expression of Connexin43 and Connexin45 in intestinal and ureteral smooth muscle contraction in mice. *Dis Model Mech* 11(2):dmm032128.

36. Stark R, Panduranga M, Carman G, Dunn JCY (2012) Development of an endoluminal intestinal lengthening capsule. *J Pediatr Surg* 47(1):136–141.

37. Mills CG, et al. (2017) Asymmetric BMP4 signalling improves the realism of kidney organoids. *Sci Rep*. doi:10.1038/s41598-017-14809-8.

38. Chevalier NR, Gazguez E, Dufour S, Fleury V (2016) Measuring the micromechanical properties

of embryonic tissues. *Methods* 94:120–128.

39. Baumann R, Meuer HJ (1992) Blood oxygen transport in the early avian embryo. *Physiol Rev* 72(4):941–965.

40. Tazawa H (1980) Oxygen and CO_2 Exchange and Acid-Base Regulation in the Avian Embryo. *Am Zool*. doi:10.2307/3882402.

41. Steven R. Schmid, Bernard J. Hamrock BOJ (2013) *Fundamentals of Machine Elements, Third Edition*.